Terahertz generation using plasmonic photoconductive gratings



2012 New J. Phys. 14 105029

(http://iopscience.iop.org/1367-2630/14/10/105029)

New Journal of Physics
The open-access journal for physics

# Terahertz generation using plasmonic photoconductive gratings

**Christopher W Berry and Mona Jarrahi**[1]
Department of Electrical Engineering and Computer Science, University of Michigan, Ann Arbor, 1301 Beal Ave, Ann Arbor, MI 48109, USA
E-mail: mjarrahi@umich.edu

*New Journal of Physics* **14** (2012) 105029 (12pp)
Received 4 June 2012
Published 30 October 2012
Online at http://www.njp.org/
doi:10.1088/1367-2630/14/10/105029

**Abstract.** A photoconductive terahertz emitter based on plasmonic contact electrode gratings is presented and experimentally demonstrated. The nanoscale grating enables ultrafast and high quantum efficiency operation simultaneously, by reducing the photo-generated carrier transport path to the photoconductor contact electrodes. The presented photoconductor eliminates the need for a short-carrier lifetime semiconductor, which limits the efficiency of conventional photoconductive terahertz emitters. Additionally, the photo-absorbing active area of the plasmonic photoconductive terahertz emitter can be increased without a significant increase in the capacitive loading to the terahertz radiating antenna, enabling high quantum-efficiency operation at high pump power levels by preventing the carrier screening effect and thermal breakdown. A plasmonic photoconductive terahertz emitter prototype based on the presented scheme is implemented and integrated with dipole antenna arrays on a semi-insulating $In_{0.53}Ga_{0.47}As$ substrate. Emitted terahertz radiation is characterized in a terahertz time-domain spectroscopy setup, measuring a terahertz pulse width of 590 fs full-width at half maximum in response to 150 fs pump pulses at 925 nm.

[1] Author to whom any correspondence should be addressed.

## Contents



## 1. Introduction

One of the most commonly used optical techniques for generating terahertz waves, by combination with RF techniques, is based on photoconduction [1]. The operation of photoconductive terahertz emitters is based on an incident optical pump generating electron–hole pairs in the photo-absorbing semiconductor region of a photoconductor. An applied voltage across the photoconductor contact electrodes drifts the generated carriers toward their corresponding contact electrodes. The collected photocurrent at the photoconductor contact electrodes drives a terahertz antenna connected to the photoconductor contact electrodes. The generated photocurrent follows the waveform of the optical pump. By using a sub-picosecond optical pulse or heterodyning two continuous-wave (CW) optical beams with a terahertz frequency difference, a pulsed or CW terahertz current is coupled to the terahertz radiating antenna, respectively. For efficient operation at terahertz frequencies, the transport time of the photo-generated carriers to the photoconductor contact electrodes should be a fraction of the oscillation period of the desired radiation [2]. Conventionally, short-carrier lifetime photo-absorbing semiconductors have been used to offer the required ultrafast carrier transport times. Reducing the contact electrode spacing of the photoconductor is an alternative method to achieve short carrier transport times. However, the significant reduction in optical pump absorption at subwavelength contact electrode spacing has prevented the effectiveness of this alternative scheme.

Technological breakthroughs in the field of solid-state and fiber lasers make photoconductive emitters very promising, enabling extreme frequency tunability and high spectral purity (required for CW terahertz generation) and broad bandwidth (required for pulsed terahertz generation) while operating at room temperature. Specifically, availability of high power (>10 W average), narrow line-width (KHz range), and wavelength tunable (10 s of nm) fiber amplifiers at 1550 nm and 1030 nm wavelengths makes photoconductive terahertz emitters pumped at these pump wavelengths very promising for future low-cost, compact and high-performance terahertz systems. The major advantage of photoconductive terahertz emitters compared to the terahertz sources based on nonlinear optical effects is that their optical-to-terahertz conversion efficiency is not restricted by the Manley–Rowe limit. This is because each absorbed photon can generate one electron–hole pair, which can emit several terahertz photons upon reaching the terahertz antenna. In other words, the power efficiency of photoconductive sources can reach 100%, orders of magnitude higher than the Manley–Rowe limit. Although the power efficiency of photoconductive emitters can theoretically exceed 100%, the low quantum efficiency of conventional ultrafast photoconductors imposes substantially lower power efficiencies.

The quantum efficiency limitation of conventional photoconductive terahertz emitters stems from the diffraction limit, requiring micrometer-scale spacing between photoconductor contact electrodes. Considering the nominal carrier drift velocity values of $\sim 10^7\,\mathrm{cm\,s^{-1}}$ in photo-absorbing semiconductors, a very small portion of the electron–hole pairs generated between the photoconductor contact electrodes can reach the terahertz radiating antenna in a sub-picosecond time scale to contribute to terahertz radiation. The rest of the carriers just contribute to the photoconductor dc current, which can significantly drop the bias field across the photoconductor active region and reduce the photo-generated carrier acceleration toward contact electrodes. Therefore, the majority of photoconductive terahertz emitters use short-carrier lifetime semiconductors to suppress the excess dc current by forcing the charge carriers with long transport times to the contact electrodes to recombine before reaching the contact electrodes. As an example, conventional photoconductive terahertz emitters based on short-carrier lifetime GaAs pumped at 850 nm use contact electrodes spacing of $\sim 2\,\mu$m to operate beyond the diffraction limit [3]. Considering the maximum carrier drift velocity of $\sim 10^7\,\mathrm{cm\,s^{-1}}$ in GaAs, only $\sim 5\%$ of the photo-generated carriers can reach the photoconductor contact electrodes within a picosecond, and the majority of the carriers get recombined inside the short-carrier lifetime substrate. Additionally, quantum efficiency of photoconductive terahertz emitters are further degraded at high pump power levels due to the carrier screening effect and thermal breakdown. Large-aperture photoconductive antennas and a variety of electrode configurations have been employed to suppress such effects and enhance the carrier accelerating field strength [4–11]. It should be noted that the optical-to-terahertz conversion efficiency has a quadratic relation with photoconductor quantum efficiency. Therefore, alternative photoconductive terahertz emitter architectures, which are not restricted by the classical diffraction limit, are crucial for development of high efficiency photoconductive terahertz emitters.

The use of short-carrier lifetime semiconductors for conventional diffraction-limited photoconductive terahertz emitters introduces a number of shortcomings that lead to further power efficiency degradation. The most commonly used short-carrier lifetime substrates for operation at ~800 nm pump wavelengths are prepared by growing GaAs at low temperatures (~200 °C) [12, 13] or introducing ErAs islands while growing GaAs [14, 15]. At 1550 and 1030 nm wavelengths where high power, tunable, narrow line-width and compact lasers are commercially available, short-carrier lifetime substrates are prepared by growing InGaAs at low temperatures [16], ion irradiation of InGaAs [17–19], or introducing ErAs islands while growing InGaAs [20, 21]. An alternative scheme is based on embedding low-temperature grown InGaAs between InAlAs layers to offer high photoconductor dark resistivity levels [22]. All of the listed techniques for developing short-carrier lifetime substrates incorporate a high density of trap sites within the semiconductor lattice and therefore degrade carrier mobility and photoconductor quantum efficiency significantly. The high density of trap sites in short-carrier lifetime semiconductors also degrades semiconductor's thermal conductivity [23], which leads to a premature thermal breakdown of photoconductors at high optical pump power levels.

To address the quantum efficiency limitation of conventional photoconductive terahertz emitters, we present a new photoconductive terahertz emitter concept which operates beyond the diffraction limit. By incorporating a plasmonic photoconductor contact electrode configuration, the average photo-generated carrier transport path to the photoconductor contact electrodes is significantly reduced compared to conventional photoconductors with micron-scale contact electrode spacings. We experimentally demonstrate that the nano-scale carrier transport path

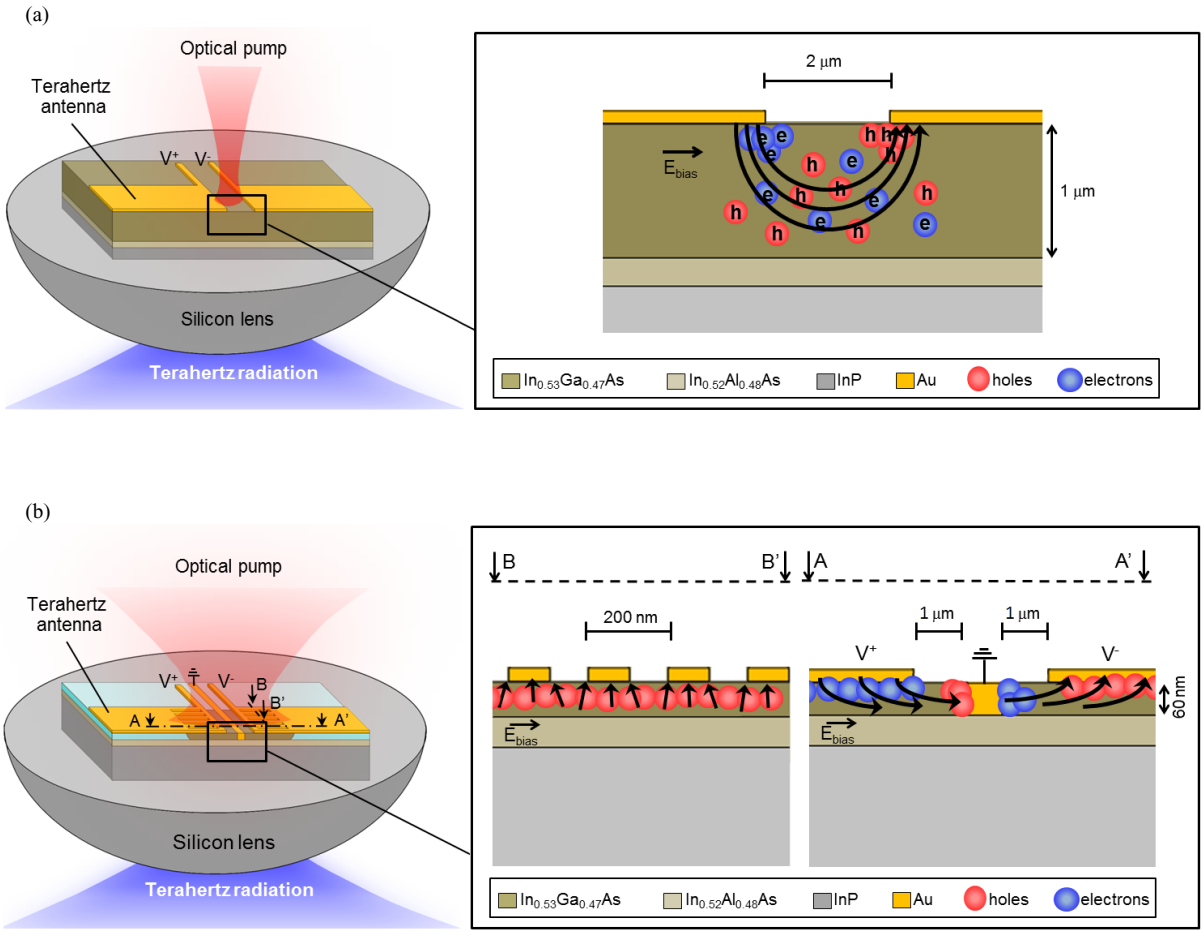


**Figure 1.** Schematic diagram and operation concept of (a) conventional photoconductive terahertz emitters based on short-carrier lifetime photo-absorbing semiconductors, and (b) the plasmonic photoconductive terahertz emitter based on nanoscale contact electrode gratings on a high-quality crystalline substrate.

lengths provided by plasmonic contact electrode gratings allow sub-picosecond photoconductor response time without using any short-carrier lifetime semiconductor. By operation beyond the diffraction limit, the presented photoconductive terahertz emitter scheme enables high quantum efficiency and ultrafast operation simultaneously and paves the way toward high optical-to-terahertz conversion efficiencies.

## 2. Device concept

Figure 1 shows the schematic diagram and operation concept of a plasmonic photoconductive terahertz emitter (figure 1(b)) in comparison with a conventional photoconductive terahertz emitter with a similar terahertz radiating antenna (figure 1(a)). The anode and cathode contact of the photoconductor consist of two arrays of nanoscale metallic gratings connected to the input port of a dipole terahertz antenna. Normally, optical transmission through subwavelength

metallic apertures is diffraction limited. However, the grating geometry can be specifically designed to allow efficient optical transmission through the subwavelength metallic gratings into the photo-absorbing active region by excitation of surface plasmon waves along the periodic metallic grating interface [24]. Instead of using an interdigitated configuration for the anode and cathode contact gratings, the contact gratings are interconnected with an overall spacing of $\sim$3 $\mu$m between the anode and cathode contacts. This maintains low capacitive loading to the terahertz radiating antenna while reducing the photo-generated carrier transport path to the contact electrodes significantly. The shortcoming of the presented contact electrode configuration is that only half of the photo-generated carriers will reach the contact electrode gratings in a sub-picosecond time scale, limiting the maximum photoconductor quantum efficiency to 50%. In order to maintain the photoconductor ultrafast operation in the absence of a short-carrier lifetime substrate, a middle ground electrode will collect the remaining holes and electrons and prevents their slow collection by the opposite anode and cathode contact electrodes. Conventional photoconductive terahertz emitters are usually fabricated on a $\sim$1 $\mu$m thick short-carrier lifetime semiconductor layer. Although only the photocarriers generated within $\sim$100 nm from the contact electrodes can be collected in a sub-picosecond time scale to contribute to terahertz radiation, excess carriers generated deeper inside the substrate would not increase photoconductor dc current due to recombination before reaching photoconductor contact electrodes. In order to maintain low photoconductor dc current levels and a sub-picosecond device response time in the absence of a short-carrier lifetime substrate, the presented plasmonic photoconductive terahertz emitter is fabricated on a photo-absorbing semiconductor layer with less than 100 nm thickness to prevent photo-carrier generation at deep semiconductor regions that do not contribute to terahertz radiation.

Interaction of the optical pump with the nanoscale contact gratings is analytically characterized and the grating structure is designed to allow ultrafast and high quantum efficiency operation simultaneously [25]. Figure 2(a) shows the designed nanoscale Au grating with 200 nm pitch, 100 nm metal width and 50 nm metal height for enhanced transmission of a TM-polarized optical pump at 800–1550 nm wavelengths into a 60 nm $In_{0.53}Ga_{0.47}As$ active layer grown on a lattice-matched $In_{0.52}Al_{0.48}As$ buffer layer on a semi-insulating InP substrate. Using a finite-element solver (COMSOL), we have analyzed the interaction of a TM-polarized optical wave with the designed Au grating at 800 and 1550 nm wavelengths. The power flow (red arrows) at the Au grating cross section shows how the propagating light bends on top of the subwavelength metallic grating to allow high efficiency transmission into the photo-absorbing substrate. It also shows that the intensity of the transmitted optical pump is significantly enhanced near the corners of the Au grating, further reducing the average transport time of the photo-generated carriers to the contact electrodes. Optical intensity enhancement near the corners of the Au grating is due to the excitation of surface plasmon waves along the periodic Au grating interface, which are constrained at the metal–dielectric interface.

The designed nanoscale Au grating offers about 60% optical transmission into the $In_{0.53}Ga_{0.47}As$ active layer at 800 and 1550 nm, bound by the Fresnel reflection at the $In_{0.53}Ga_{0.47}As$–air interface. However, the optical intensity in close proximity to the Au gratings is about an order of magnitude higher at a wavelength of 800 nm, compared to 1550 nm (figure 2(b)). This confirms the role of surface plasmon waves in enhancing the optical intensity near the Au gratings, in spite of the fact that much stronger intensity enhancement levels could be achieved at shorter optical wavelengths [26]. It should be noted that the excited surface plasmon waves are tightly confined to the Au interface. Therefore, the thin adhesion layers

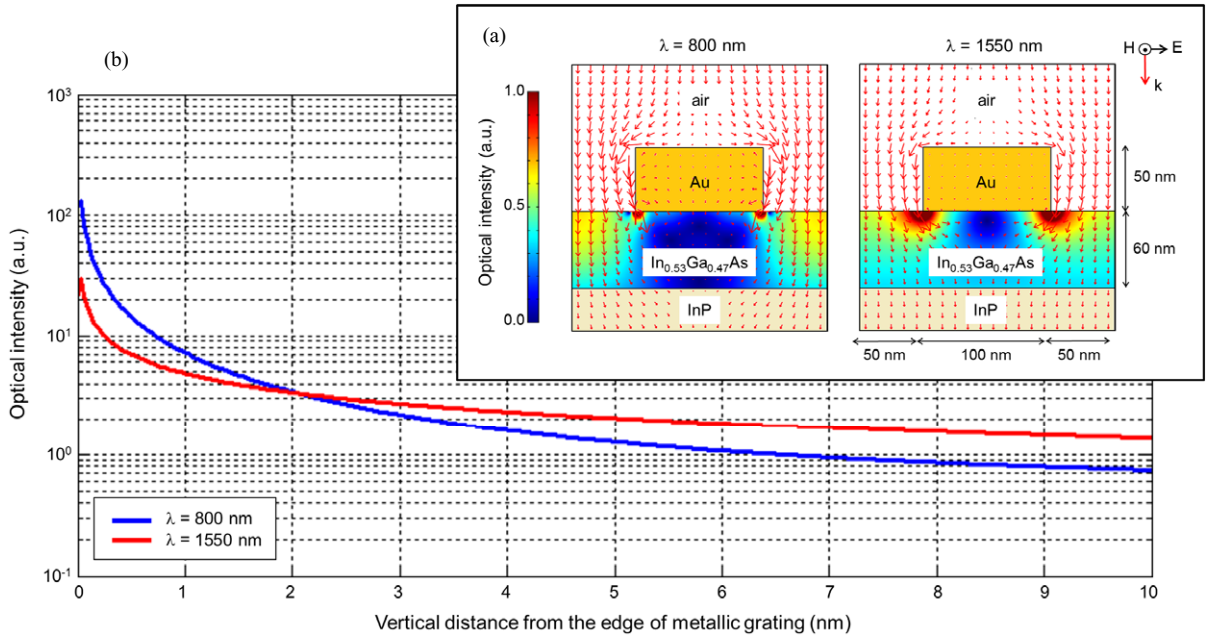


**Figure 2.** (a) Interaction of a TM-polarized optical beam with the designed Au grating at 800 and 1550 nm. Red arrows and color-map show the optical power flow and intensity inside the $In_{0.53}Ga_{0.47}As$ active layer, respectively. (b) Optical intensity variation as a function of vertical distance from the edge of Au gratings, indicating the tightly confined surface plasmon waves at the Au-$In_{0.53}Ga_{0.47}As$ interface.

(e.g. Titanium) often used for facilitating Au liftoff in practical applications would have a negative impact on the discussed plasmonic enhancement.

The impulse response of the designed plasmonic photoconductor is estimated by calculating the photo-generated carrier profile and the applied bias electric field in a multi-physics finite-element solver (COMSOL). The bias voltage is set to limit the maximum induced electric field to half of the breakdown field in $In_{0.53}Ga_{0.47}As$. Figure 3 shows the induced electric field and the corresponding electron drift velocity inside the 60 nm thick $In_{0.53}Ga_{0.47}As$ layer as a function of distance from the ground electrode. In spite of the rapid reduction of the induced electric field as a function of distance from the ground electrode (figure 3(a)), electron drift velocity exhibits a much more gradual reduction as a function of distance from the ground electrode (figure 3(b)). This is because the carrier drift velocity does not have a linear dependence on the applied electric field at high field intensities and saturates due to carrier scattering inside the semiconductor lattice [27–29]. As illustrated in figure 3(b), electron drift velocity in $In_{0.53}Ga_{0.47}As$ remains above $0.5 \times 10^7\,\mathrm{cm\,s^{-1}}$ while reducing the bias electric field from 100 to $0.4\,\mathrm{kV\,cm^{-1}}$ at either side of a $20\,\mu\mathrm{m}$ long plasmonic contact electrode grating [27–29]. It should be mentioned that the drift velocity of photo-generated holes is much smaller than photo-generated electrons even at high field intensities (figure 3(b)). This makes electrons the dominant contributor to photoconductor impulse response, similar to conventional photoconductive sources. Therefore, the nonlinear dependence of carrier drift velocity on the applied electric field allows use of relatively large photoconductor active areas with plasmonic

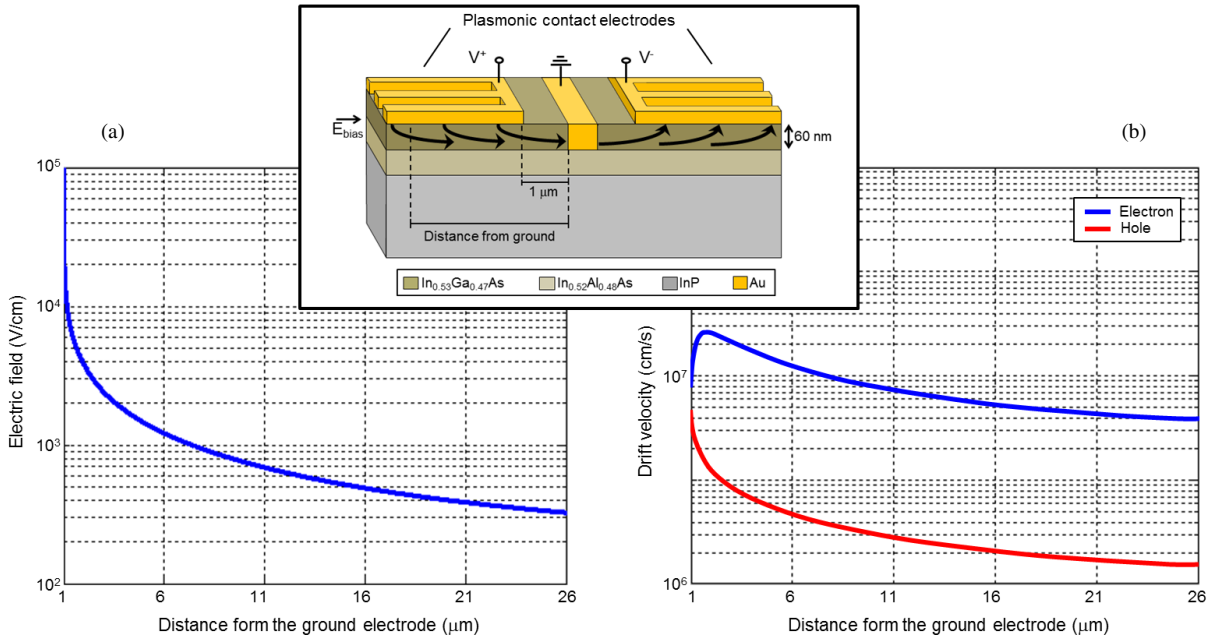


**Figure 3.** (a) Induced electric field inside the $In_{0.53}Ga_{0.47}As$ layer as a function of distance from the ground electrode. The bias voltage is set to produce a maximum electric field of $10^5\,V\,cm^{-1}$ (half of the $In_{0.53}Ga_{0.47}As$ breakdown field). (b) Estimated carrier drift velocity inside the $In_{0.53}Ga_{0.47}As$ layer as a function of distance from the ground electrode by using the reported carrier drift velocity in $In_{0.53}Ga_{0.47}As$ as a function of the applied electric field [27–29].

contact electrodes without a significant reduction in the carrier drift velocity and photoconductor efficiency. The impulse response of the designed plasmonic photoconductor to a TM-polarized optical impulse is estimated by calculating the collected transient photocurrent at the contact electrodes under the influence of the induced bias electric field along a 20 $\mu$m long plasmonic contact electrode [30]. For this purpose, the photo-generated carrier density is derived from the calculated optical intensity in the $In_{0.53}Ga_{0.47}As$ active layer and combined with the electric field data in the classical drift-diffusion model to calculate the induced photocurrent.

We have analyzed the impulse response of the designed plasmonic photoconductor at 925 nm pump wavelength in comparison with a conventional photoconductor with interdigitated Au contact electrodes (100 nm width and 2 $\mu$m pitch) fabricated on a short-carrier lifetime $In_{0.53}Ga_{0.47}As$ substrate with a carrier lifetime of 0.3 ps. The bias voltage in both cases is set to limit the maximum induced electric field to half of the breakdown field in $In_{0.53}Ga_{0.47}As$. The 925 nm pump wavelength is the highest wavelength supported by the Ti : sapphire mode-locked laser available in our lab, which is used to characterize the ultrafast response of the fabricated plasmonic photoconductive emitter prototypes. The results are presented in figure 4(a), indicating the superior performance of the designed plasmonic photoconductor offering high-quantum efficiency and ultrafast operation simultaneously. The advantage of the designed plasmonic photoconductor is more apparent when comparing its responsivity with the conventional photoconductor fabricated on a short-carrier lifetime $In_{0.53}Ga_{0.47}As$ substrate. The responsivity spectra are calculated by convolving the impulse response of photoconductors with

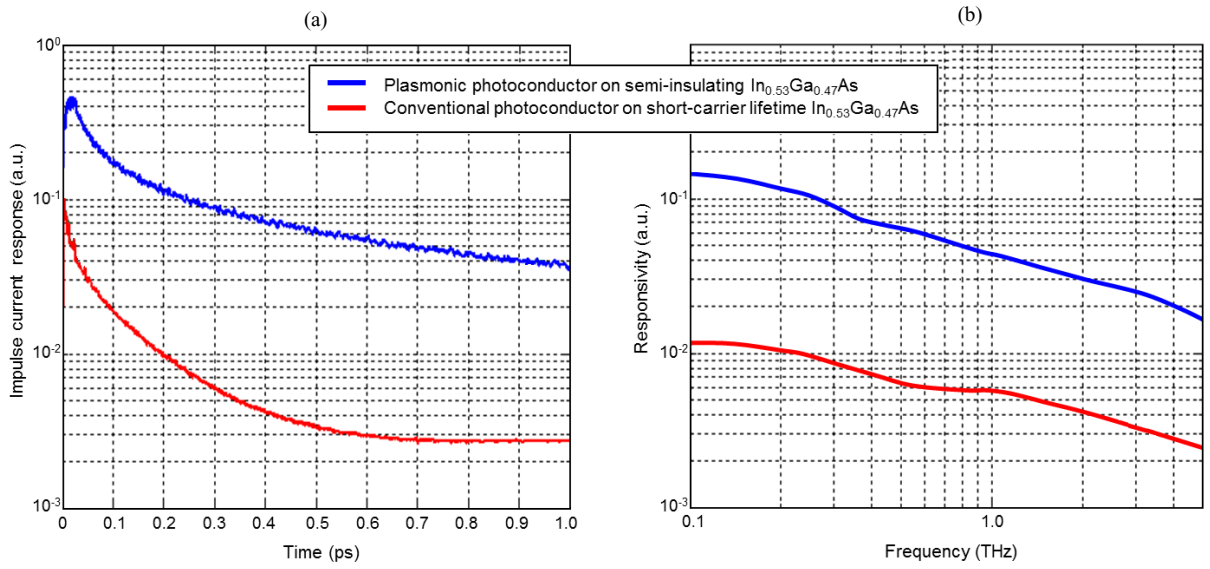


**Figure 4.** (a) Calculated impulse current response and (b) responsivity spectrum of the designed plasmonic photoconductor (with 200 nm pitch, 100 nm width and 50 nm thick Au contact gratings fabricated on a 60 nm thick $In_{0.53}Ga_{0.47}As$ active layer) in comparison with a conventional photoconductor with interdigitated Au contact gratings (with 100 nm width and 2 $\mu$m pitch fabricated on a short-carrier lifetime $In_{0.53}Ga_{0.47}As$ substrate with a carrier lifetime of 0.3 ps) at 925 nm pump wavelength.

the sinusoidal power envelope of two frequency-offset optical beams as a function of optical beat frequency. The responsivity spectra (figure 4(b)) indicate that the designed plasmonic photoconductor offers an order of magnitude higher responsivity levels compared with the conventional photoconductor fabricated on a short-carrier lifetime $In_{0.53}Ga_{0.47}As$ substrate.

It should be mentioned that at a given pump power, the radiated power from a photoconductive terahertz emitter has a quadratic dependence on the photoconductor responsivity. Therefore, compared with the conventional photoconductors, the designed plasmonic photoconductor offers two orders of magnitude higher optical-to-terahertz conversion efficiencies. An additional advantage of the designed plasmonic photoconductor compared with conventional photoconductor designs is that the photoconductor active area along the antenna input ports can be increased without substantial increase in capacitive loading to the antenna. For example, in order to induce the same capacitive loading to terahertz radiating antenna, the photo-absorbing active area of the designed plasmonic photoconductor would be 20 times larger than the active area of the discussed conventional photoconductor. This makes plasmonic photoconductive sources very attractive for operating at high pump power levels, where maximum radiated power of conventional designs is limited by the carrier screening effect and thermal breakdown.

## 3. Experimental results and discussion

For the first generation plasmonic photoconductive terahertz emitters, the designed Au contact gratings are integrated as a part of densely spaced dipole antennas. The array of closely spaced

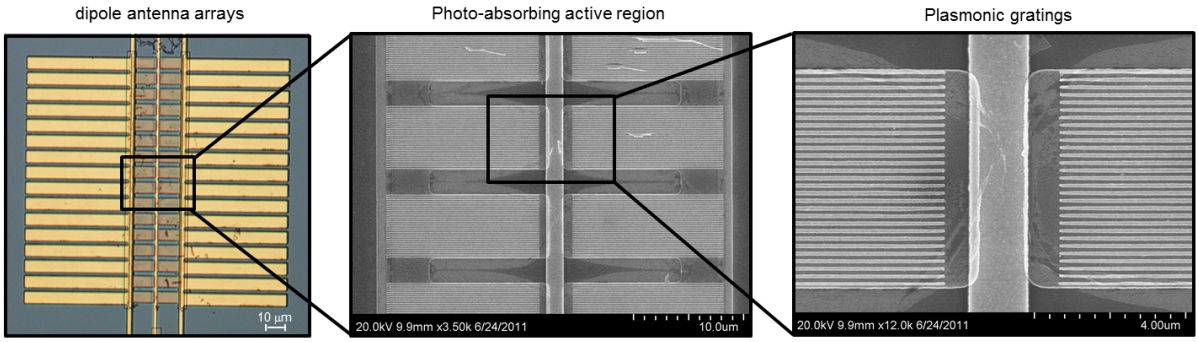


**Figure 5.** SEM image of a plasmonic photoconductive terahertz emitter prototype based on nanoscale Au contact electrode gratings and 6 $\mu$m wide, 130 $\mu$m long dipole antenna arrays.

dipole antennas is designed to increase the photoconductor active area while maintaining a small RC time-constant and high radiation resistance. We have used ADS and HFSS software packages to optimize the antenna array structure for maximum radiation power, by combining the antenna radiation parameters, photoconductor parasitics, and the amount of injected current based on photoconductor active area [31, 32]. Arrays of 2–10 $\mu$m wide dipole antennas with lengths varying between 130 and 260 $\mu$m and separated laterally by 2 $\mu$m are selected for the prototype devices.

Following our analytical modeling, plasmonic photoconductive emitter prototypes were fabricated on a 60 nm thick un-doped $In_{0.53}Ga_{0.47}As$ layer, epitaxially grown on a lattice-matched un-doped $In_{0.52}Al_{0.48}As$ buffer layer on a semi-insulating InP substrate (figure 5). The un-doped $In_{0.53}Ga_{0.47}As$ and $In_{0.52}Al_{0.48}As$ layers together with the 500 $\mu$m thick semi-insulating InP substrate would introduce a negligible absorption loss at terahertz frequencies. Nanoscale contact gratings were patterned using electron-beam lithography followed by Ti/Au (3 nm/50 nm) deposition and liftoff. The $In_{0.53}Ga_{0.47}As$ layer is etched away from the regions outside the photoconductor active area to reduce the background photocurrent that does not contribute to terahertz radiation. Dipole antenna arrays are patterned using optical lithography on a 150 nm thick $SiO_2$ layer deposited on $In_{0.53}Ga_{0.47}As$ to reduce antenna losses on the low-resistivity $In_{0.53}Ga_{0.47}As$ substrate.

The ultrafast operation of the plasmonic photoconductive emitter prototypes is confirmed by characterizing their radiation in a time-domain spectroscopy setup pumped by a mode-locked Ti : sapphire laser providing 150 fs pump pulses at 925 nm center wavelength with a 76 MHz repetition rate. An electro-optic sampling detection scheme using a ZnTe crystal is used to detect the radiated electric field. Figure 6(a) shows the measured time-domain radiation of a plasmonic photoconductive emitter prototype with an antenna length of 260 $\mu$m. A 590 fs full-width at half maximum is measured in the time domain, showing the ultrafast response of the device without using a short-carrier lifetime semiconductor. The 590 fs wide radiation peak is followed by the resonant response of the 260 $\mu$m long dipole antenna. Figure 6(b) shows the corresponding frequency-domain radiation from the plasmonic photoconductive emitter prototype, indicating a terahertz radiation bandwidth of more than 1.5 THz. The radiation peak at 0.25 THz is associated with the resonance peak of the dipole antenna of the characterized prototype.

Radiated power from the plasmonic photoconductive emitter prototypes are measured by using a pyroelectric detector (Spectrum Detector Inc., SPI-A-65 THz). A 5 Hz modulation

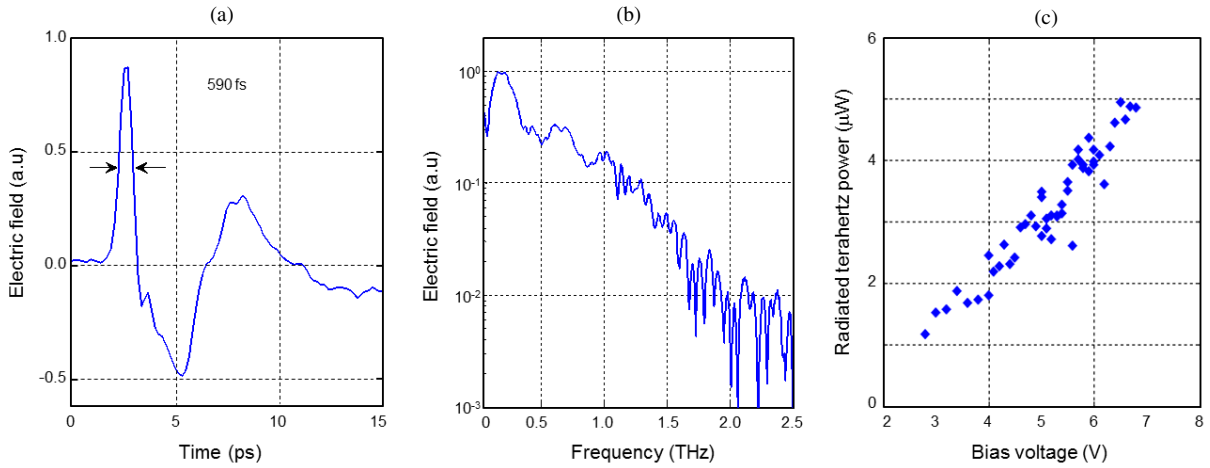


**Figure 6.** Measured radiation from a fabricated plasmonic photoconductive terahertz emitter prototype with a dipole antenna length of 260 $\mu$m in a time-domain spectroscopy setup. The time domain and frequency domain radiated field are shown in (a) and (b), the measured radiated power under an optical pump illumination of 85 mW and as a function of the bias voltage is shown in (c).

required by the pyroelectric detector was provided by an optical chopper in the optical pump path. The modulated radiation was measured with a lock-in amplifier and converted to terahertz power by using the pyroelectric detector responsivity in the 0.1–2.5 THz frequency range. Figure 6(c) shows the measured radiated power from a plasmonic photoconductive emitter prototype with antenna length of 260 $\mu$m, under an optical pump illumination of 85 mW and as a function of the bias voltage. The linear dependence of the radiated terahertz power and bias voltage indicates the insufficient induced electric field for efficient acceleration of the photo-generated carriers. This limitation is associated with the low bandgap energy of InGaAs, leading to high dark current levels. Under this constraint, a radiated power of 5 $\mu$W is measured for the plasmonic photoconductive terahertz emitter prototype at a bias voltage of 6.5 V. It should be mentioned that the high dark current associated with the low bandgap energy of InGaAs has been the major obstacle for InGaAs-based photoconductive emitters. There have been extensive studies on various techniques to mitigate this challenge [17–19] and very promising solutions have been offered for reducing photoconductor dark current by embedding InGaAs between InAlAs trapping layers [10, 22]. Although the output power of the presented plasmonic photoconductive terahertz emitter can be further enhanced using high resistivity photo-absorbing substrates, its maximum output power in the absence of such high resistivity photo-absorbing substrates is 50 times higher than previously demonstrated photoconductive emitters with planar dipole antennas fabricated on high resistivity InGaAs/InAlAs photo-absorbing layers [10].

## 4. Conclusion

In summary, a photoconductive terahertz emitter based on plasmonic contact electrodes is presented for the first time and characterized experimentally. The nano-scale carrier transport

path lengths provided by plasmonic contact electrode gratings allow high quantum efficiency and ultrafast operation simultaneously. It also eliminates the need to use short-carrier lifetime substrates which are a major source of quantum efficiency degradation in conventional photoconductors. Additionally, the photo-absorbing active area of plasmonic photoconductive terahertz emitters can be increased without a significant increase in the capacitive loading to the terahertz radiating antenna. This allows high quantum-efficiency operation at high pump power levels by preventing the carrier screening effect and thermal breakdown. The presented plasmonic photoconductive terahertz emitter would benefit from high-aspect ratio nano-scale contact electrodes embedded inside the substrate [33–36], which enable a significant increase in optical-to-terahertz conversion efficiency by ultrafast collection of photo-generated carriers in deeper substrate regions.

## Acknowledgments

The authors gratefully acknowledge the financial support from DARPA Young Faculty Award (N66001-10-1-4027), NSF CAREER Award (ECCS-1054454) and Office of Naval Research (N00014-11-1-0096).

## References

[1] Auston D H, Cheung K P and Smith P R 1984 Picosecond photocoducting Hertzian dipoles *Appl. Phys. Lett.* **45** 284–6

[2] Preu S, Dohler G H, Malzer S, Wang L J and Gossard A C 2011 Tunable, continuous-wave terahertz photomixer sources and applications *J. Appl. Phys.* **109** 061301

[3] Bjarnason J E, Chan T L J, Lee A W M, Brown E R, Driscoll D C, Hanson M, Gossard A C and Muller R E 2004 ErAs:GaAs photomixer with two-decade tunability and 12 $\mu$W peak output power *Appl. Phys. Lett.* **85** 3983–5

[4] Awad M, Nagel M, Kurz H, Herfort J and Ploog K 2007 Characterization of low temperature GaAs antenna array terahertz emitters *Appl. Phys. Lett.* **91** 181124

[5] Beck M, Schafer H, Klatt G, Demsar J, Winnerl S, Helm M and Dekorsy T 2010 Impulsive terahertz radiation with high electric fields from an amplifier-driven large-area photoconductive antenna *Opt. Express* **18** 9251–7

[6] Jarrahi M and Lee T H 2008 High power tunable terahertz generation based on photoconductive antenna arrays *Proc. IEEE MTT-S Int. Microw. Symp. Dig.* pp 391–4

[7] Jarrahi M 2009 Terahertz radiation-band engineering through spatial beam-shaping *Photon. Technol. Lett.* **21** 830–2

[8] Hattori T, Egawa K, Ookuma S I and Itatani T 2006 Intense terahertz pulses from large-aperture antenna with interdigitated electrodes *Japan. J. Appl. Phys.* **45** L422–4

[9] Kim J H, Polley A and Ralph S E 2005 Efficient photoconductive terahertz source using line excitation *Opt. Lett.* **30** 2490–92

[10] Roehle H, Dietz R J B, Hensel H J, Böttcher J, Künzel H, Stanze D, Schell M and Sartorius B 2010 Next generation 1.5 $\mu$m terahertz antennas: mesa-structuring of InGaAs/InAlAs photoconductive layers *Opt. Express* **18** 2296–301

[11] Taylor Z D, Brown E R, Bjarnason J E, Hanson M P and Gossard A C 2006 Resonant-optical-cavity photoconductive switch with 0.5% conversion efficiency and 1.0 W peak power *Opt. Lett.* **31** 1729–31

[12] Warren A C, Katzenellenbogen N, Grischkowsky D, Woodall J M, Melloch M R and Otsuka N 1991 Subpicosecond, freely propagating electromagnetic pulse generation and detection using GaAs:As epilayers *Appl. Phys. Lett* **58** 1512–4

[13] Shen Y C, Upadhya P C, Beere H E, Linfield E H, Davies A G, Gregory I S, Baker C, Tribe W R and Evans M J 2004 Generation and detection of ultrabroadband terahertz radiation using photoconductive emitters and receivers *Appl. Phys. Lett.* **85** 164–6

[14] Kadow C, Fleischer S B, Ibbetson J P, Bowers J E, Gossard A C, Dong J W and Palmstrom C J 1999 Self-assembled ErAs islands in GaAs: growth and subpicosecond carrier dynamics *Appl. Phys. Lett.* **75** 3548–50

[15] Griebel M, Smet J H, Driscoll D C, Kuhl J, Alvarez Diez C, Freytag N, Kadow C, Gossard A C and von Klitzing K 2003 Tunable subpicosecond optoelectronic transduction in superlattices of self-assembled ErAs nanoislands *Nature Mater.* **2** 122–6

[16] Takahashi R, Kawamura Y, Kagawa T and Iwamura H 1994 Ultrafast 1.55 $\mu$m photoresponses in low-temperature-grown InGaAs/InAlAs quantum wells *Appl. Phys. Lett.* **65** 1790–2

[17] Mangeney J, Chimot N, Meignien L, Zerounian N, Crozat P, Blary K, Lampin J F and Mounaix P 2007 Emission characteristics of ion-irradiated $In_{0.53}Ga_{0.47}As$ based photoconductive antennas excited at 1.55 $\mu$m *Opt. Express* **15** 8943–50

[18] Carmody C, Tan H H, Jagadish C, Gaarder A and Marcinkevičius S 2003 Ion-implanted $In_{0.53}Ga_{0.47}As$ for ultrafast optoelectronic applications *Appl. Phys. Lett.* **82** 3913–5

[19] Suzuki M and Tonouchi M 2005 Fe-implanted InGaAs terahertz emitters for 1.56 $\mu$m wavelength excitation *Appl. Phys. Lett.* **86** 051104

[20] Driscoll D C, Hanson M P, Gossard A C and Brown E R 2005 Ultrafast photoresponse at 1.55 $\mu$m in InGaAs with embedded semimetallic ErAs nanoparticles *Appl. Phys. Lett.* **86** 051908

[21] Ospald F, Maryenko D, von Klitzing K, Driscoll D C, Hanson M P, Lu H, Gossard A C and Smet J H 2008 1.55 $\mu$m ultrafast photoconductive switches based on ErAs:InGaAs *Appl. Phys. Lett.* **92** 131117

[22] Sartorius B, Roehle H, Künzel H, Böttcher J, Schlak M, Stanze D, Venghaus H and Schell M 2008 All-fiber terahertz time-domain spectrometer operating at 1.5 $\mu$m telecom wavelengths *Opt. Express* **16** 9565–70

[23] Jackson A W, Ibbetson J P, Gossard A C and Mishra U K 1999 Reduced thermal conductivity in low-temperature grown GaAs *Appl. Phys. Lett.* **74** 2325–7

[24] Berry C W and Jarrahi M 2010 Plasmonically-enhanced localization of light into photoconductive antennas *Proc. Conf. of Lasers and Electro-Optics (San Jose, CA, 16–21 May 2010)* CFI2

[25] Berry C W and Jarrahi M 2012 Plasmonic photoconductive terahertz emitters based on nanoscale gratings *Proc. Conf. of Lasers and Electro-Optics (San Jose, CA, 6–11 May 2010)* CF2M.1

[26] Staffaroni M, Conway J, Vedantam S, Tang J and Yablonovitch E 2010 Circuit analysis in metal-optics arXiv:1006.3126[physics.optics]

[27] Balynas V, Krotkus A, Stalnionis A, Gorelionok A T, Shmidt N M and Tellefsen J A 1990 Time-resolved, hot-electron conductivity measurement using an electro-optic sampling technique *Appl. Phys.* A **51** 357–60

[28] Ahmed S R, Nag B R and Roy M D 1985 Hot-electron transport in $In_{0.53}Ga_{0.47}As$ *Solid State Electron.* **28** 1193–7

[29] Adachi S 1992 *Physical Properties of III-Y Semiconductor Compounds* (New York: Wiley)

[30] Berry C W and Jarrahi M 2011 Ultrafast photoconductors based on plasmonic gratings *Proc. Int. Conf. on Infrared, Millimeter, and Terahertz Waves (Houston, TX, 2–7 October 2011)* pp 1–2

[31] Berry C W and Jarrahi M 2012 High-performance photoconductive terahertz sources based on nanoscale contact electrode gratings *IEEE Int. Microwave Symp. Digest (Montreal, Canada, 17–22 June 2012)* pp 1–3

[32] Berry C W and Jarrahi M 2012 Plasmonic photoconductive antennas for high power terahertz generation *Proc. IEEE Int. Antennas and Propagation Symp. (Chicago, IL, 8–14 July 2012)* pp 1–2

[33] Hsieh B-Y and Jarrahi M 2011 Analysis of periodic metallic nano-slits for efficient interaction of terahertz and optical waves at nano-scale dimensions *J. Appl. Phys.* **109** 084326

[34] Hsieh B-Y, Wang N and Jarrahi M 2011 Toward ultrafast pump-probe measurements at the nanoscale *Spec. Issue 'Optics in 2011' Opt. Photon. News* **22** 48

[35] Hsieh B-Y and Jarrahi M 2011 Simultaneous focusing of terahertz and optical waves into nano-scale *Proc. Int. Conf. on Infrared, Millimeter, and Terahertz Waves (Houston, TX, 2–7 October 2011)* pp 1–2

[36] Jarrahi M 2011 Extraordinary interaction of terahertz and optical waves through metallic nano-slits *Proc. URSI General Assembly and Scientific Symp. (Istanbul, Turkey, 13–20 August 2011)* pp 1–4